The V1–V2–V3 complex: quasiconformal dipole maps in primate striate and extra-striate cortex [1,2]

Mukund Balasubramanian [a] Jonathan Polimeni [b]
Eric L. Schwartz [a,*]

[a] *Department of Cognitive and Neural Systems, Boston University, 677 Beacon St. Boston, MA 02215, USA*

[b] *Department of Electrical and Computer Engineering, Boston University, 8 St. Mary's St., Boston, MA 02215, USA*

Abstract

The mapping function $w = k \log(z + a)$ is a widely accepted approximation to the topographic structure of primate V1 foveal and parafoveal regions. A better model, at the cost of an additional parameter, captures the full field topographic map in terms of the *dipole map* function $w = k \log[(z + a)/(z + b)]$. However, neither model describes topographic shear since they are both explicitly complex-analytic or conformal. In this paper, we adopt a simple *ansatz* for topographic shear in V1, V2, and V3 that assumes that cortical topographic shear is rotational, i.e. a compression along iso-eccentricity contours. We model the constant rotational shear with a quasiconformal mapping, the *wedge mapping*. Composing this wedge mapping with the dipole mapping provides an approximation to V1, V2, and V3 topographic structure, effectively unifying all three areas into a single V1–V2–V3 *complex* using five independent parameters. This work represents the first full-field, multi-area, quasiconformal model of striate and extra-striate topographic map structure.

Key words: topography, visuotopy, primary visual cortex (V1), striate cortex, extra-striate cortex, quasiconformal mapping, topographic shear, models of visual cortex

* Corresponding author.
URL: `http://www.cns.bu.edu/~eric` (Eric L. Schwartz).

[1] Supported by ONR MURI N00014-01-1-0624.

[2] This version was published in *Neural Networks*, 15(10):1157–1163, 2002.

1 Introduction

Primate visual cortex contains multiple topographic maps of the visual hemifield that are 'continuous': neighboring points in the visual field project to neighboring points in the cortex. The *cortical magnification factor* was defined by Daniel and Whitteridge (1961) to be the distance in cortex (in millimeters) devoted to representing a step of 1° in visual space. If the mapping function is complex-analytic, then the magnification factor represents the magnitude of the derivative of the mapping.

In recent years, there have been several functional magnetic resonance imaging (fMRI) studies of visual topography, or *visuotopy*. These studies have not only provided a method to non-invasively identify the borders of several visual cortical areas (Sereno et al., 1995; DeYoe et al., 1996), but have also provided a means to estimate the spatial precision of fMRI (Engel et al., 1997). Since topography is the most direct and unequivocal fMRI measurement for visual cortex, it is of importance for the purpose of validating, calibrating, and extending fMRI technology. Thus, both applied studies involving brain imaging and basic scientific studies of visual processing would benefit from a simple model of striate and extra-striate topography.

It has been reported that in area V1 the cortical magnification is either *isotropic*, i.e. locally invariant to the direction of the step in visual space (Daniel and Whitteridge, 1961; Dow et al., 1985), or approximately isotropic (Schwartz, 1985; Tootell et al., 1985; van Essen et al., 1984). Complex-analytic functions, whose derivatives are isotropic, represent *conformal mappings* wherever the derivative is non-zero, i.e. they are mappings that locally preserve angles. Therefore it is natural to consider conformal mappings as approximations to V1 topography (Schwartz, 1977, 1980). Although the mapping function corresponding to cortical visuotopy has proved to be largely conformal, there exist significant deviations in the topographic mapping from pure conformality. This deviation manifests itself as a topographic anisotropy, or *shear*.

The goal of this paper is to introduce quasiconformal methods for modeling the topography of visual cortex. Our model, called the wedge–dipole model, incorporates a simplifying assumption of uniform shear throughout a given cortical area. In addition, the wedge–dipole mapping embodies a unified model for the topography of the full visual field in areas V1, V2, and V3.

2 Review of previous models of cortical topography

2.1 The monopole mapping

The reciprocal of the V1 magnification factor has been reported to be approximately linear (Schwartz, 1977; Wilson et al., 1990; Schwartz, 1994). The complex logarithm, $w = \log(z)$, with z restricted to the half-disc,[3] is therefore an obvious candidate to model the two-dimensional structure of the mapping, as the magnitude of its derivative is inverse-linear. However, the complex logarithm has a singularity at the point $z = 0$. One can remove the singular point from the mapping domain by choosing the function $w = k\log(z + a)$, which places the singularity at $z = -a$ (see Fig. 1(b)). This function is the electrostatic complex potential *in two dimensions* of a single charge located at $z = -a$ (Needham, 1997), and therefore we refer to it as the *a-monopole mapping* (henceforth simply the *monopole mapping*). The monopole mapping captures the approximate shape of flattened V1, as well as the internal details of the topography (Schwartz, 1977, 1980). However, it does not adequately capture the far peripheral data where the inverse magnification factor is sub-linear (Schwartz, 1984), nor does it capture the shape of the far peripheral field representation in flattened V1 (e.g. compare Fig. 1(b) and (c)).

2.2 The dipole mapping

The complex potential of a pair of opposite charges (a dipole) is given by the sum of two oppositely charged monopole potentials: $w = \log(z+a) - \log(z+b)$, where the positive charge is at $z = -a$ and the negative at $z = -b$. We shall refer to this function as the *near-field ab-dipole mapping*[4] (henceforth the *dipole mapping*). The monopole potential may be considered as a special case of the dipole for which $b = \infty$. The second parameter b captures the shape of the V1 boundary exhibited at the peripheral representation (see Fig. 1(c)), as well as the fact that inverse cortical magnification factor is sub-linear in the peripheral field (Schwartz, 1983, 1984), and thus provides a two parameter approximation of the *full-field* topography of V1.

[3] The opposite hemi-field can be symmetrically represented by $w = 2\log(a) - \log(-z + a)$ for $\mathrm{Re}\{z\} \leq 0$, as in (Rojer and Schwartz, 1990), with an analogous construction for the dipole map.

[4] The term *near-field* emphasizes that we are examining the dipole field in the region *between* the charges, not the usual *far-field* dipole familiar in electrostatics, which considers the distance between the charges to approach zero.

2.3 Numerical conformal mapping

The monopole and dipole maps are examples of closed-form expressions for conformal mappings. A more general conformal model is obtained by *numerical* conformal mapping, as demonstrated by Frederick and Schwartz (1990); Schwartz (1994). In this work, the border of area V1 was computed via quasi-isometric brain flattening (Wolfson and Schwartz, 1989). Given a boundary specification, a single point correspondence, and an orientation, the Riemann mapping theorem guarantees the existence and uniqueness of a conformal mapping to the unit disc (Ahlfors, 1966a), which can be carried through to the visual hemi-field. The Symm algorithm (Symm, 1966) was then used to compute the V1 mapping, where the cortical representation of the blind spot provided the point correspondence and orientation. The result is in good agreement with 2DG data, with the typical error in the range of 10% of the linear dimensions of V1 (see Schwartz, 1994).

2.4 Topographic shear

Considerable shear has been observed near the vertical meridian representation of V1 (e.g. Blasdel and Campbell, 2001). Furthermore, a large amount of shear has been reported in V2 (Rosa et al., 1988). In the following section, we present a model that assumes a very simple form of shear: a constant, compressive shear prescribed along the iso-eccentricity curves in each area. This shear model is consistent with reports that the V2 magnification factor measured perpendicular to the V1–V2 border is much smaller (between $3:1$ and $6:1$) than that measured in the parallel direction (Roe and Ts'o, 1998).

We treat this simple form of shear as an ansatz (i.e. a preliminary working hypothesis). In Section 4, we discuss the replacement of this type of shear with more realistic ideas that incorporate known information about topographic shear.

3 Modeling topography of visual cortex

3.1 Model goals

Our goals in modeling the topography of areas V1, V2, and V3 are as follows:

(1) the maps must account for shear in V1, V2 and V3;

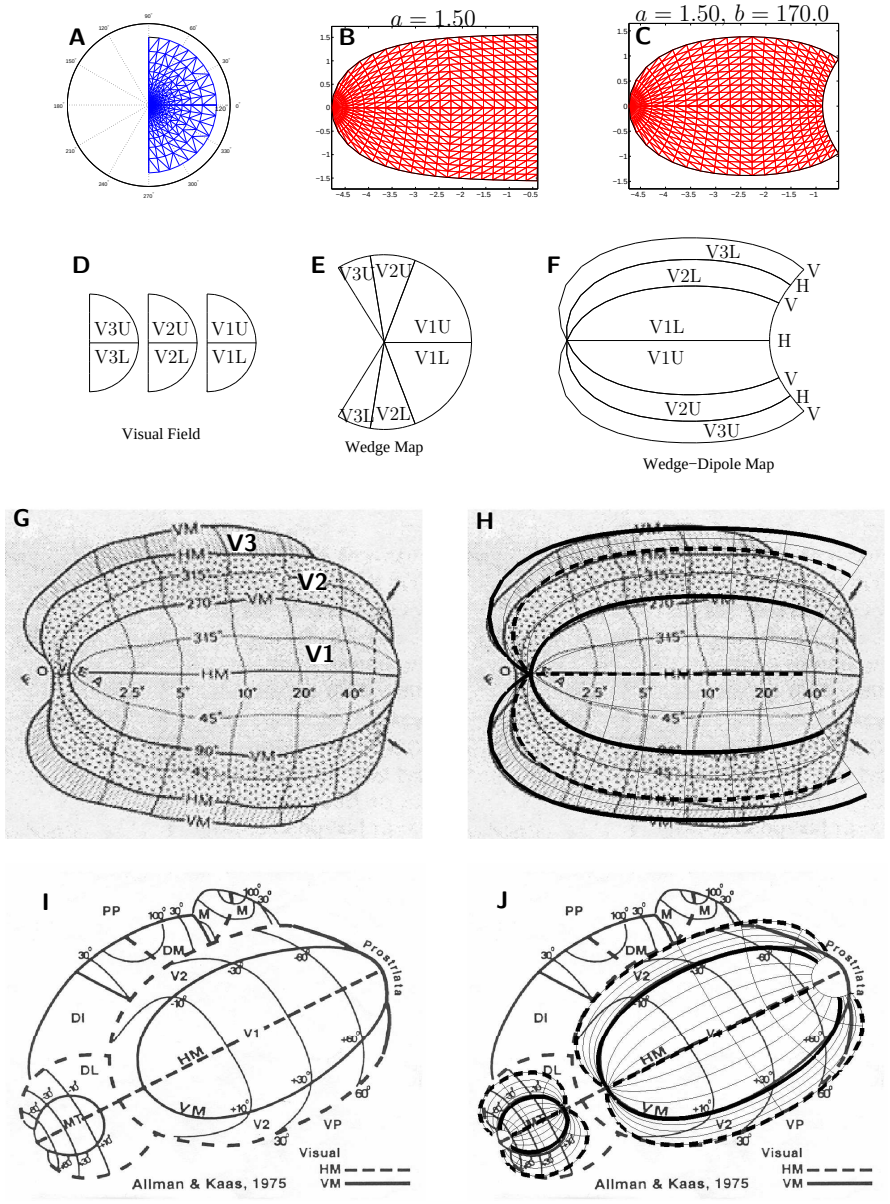

Fig. 1. (a) The right visual hemi-field. (b) The a-monopole map of the right visual hemi-field. (c) The near-field ab-dipole map of the right visual hemi-field. (d) Three copies of the visual field (one each for V1, V2, and V3) are mapped into the wedges shown in (e), by the wedge map. The near-field ab-dipole map is then applied to the wedges, resulting in the full wedge–dipole map, shown in (f). The topography of human visual areas V1, V2, and V3 is semi-qualitatively shown in (g) (Horton and Hoyt, 1991), where HM and VM mark the horizontal and vertical meridians, respectively. The wedge–dipole model superimposed on this data is shown in (h). The model parameters used here were $a = 0.9$, $b = 180$, $\alpha_1 = 0.95$, $\alpha_2 = 0.5$, and $\alpha_3 = 0.2$. The topography of owl monkey visual cortex is shown in (i) (Allman and Kaas, 1975). *Two* wedge–dipole maps are shown superimposed on this data in (j), one for the V1–V2 complex (model parameters $a = 0.8$, $b = 85$, $\alpha_1 = 1.05$, and $\alpha_2 = 0.33$), and one for the MT–DL complex (model parameters $a = 10$, $b = 70$, $\alpha_1 = 1$, and $\alpha_2 = 0.5$). The MT–DL model has been scaled by a factor of 0.65 relative to the V1–V2 model.

(2) the model must match the global shapes of areas V1, V2, and V3 as well as their relative surface areas;
(3) adjacent topographic areas must exhibit boundary conditions such that V1 and V2 share a boundary along the vertical meridian representation, and V2 and V3 share a boundary along the horizontal meridian representation (see Fig. 1(g));
(4) the Jacobian of the topographic map must reverse sign across the boundaries between V1, V2, and V3, exhibiting the *field reversal* property described in Sereno et al. (1995);
(5) the iso-eccentricity lines must be spaced approximately logarithmically.

We now present the wedge–dipole map, which provides a unified model of V1, V2, and V3 that meets the stated goals.

3.2 The wedge–dipole model

We can represent any point in the visual hemi-field with the complex variable $z = re^{i\theta}$, where r represents eccentricity and θ represents polar angle. The *wedge map* for Vk, $k = 1, 2, 3$, is the map

$$\Lambda_k(re^{i\theta}) = re^{i\Theta_k(\theta)}, \tag{1}$$

where the function Θ_1 for V1 is given by

$$\Theta_1(\theta) = \alpha_1\theta, \tag{2}$$

the function Θ_2 for V2 is given by [5]

$$\Theta_2(\theta) = \begin{cases} -\alpha_2\left(\theta - \dfrac{\pi}{2}\right) + \Theta_1\left(+\dfrac{\pi}{2}\right) & \text{if } 0^+ \le \theta \le \dfrac{\pi}{2}, \\ -\alpha_2\left(\theta + \dfrac{\pi}{2}\right) + \Theta_1\left(-\dfrac{\pi}{2}\right) & \text{if } -\dfrac{\pi}{2} \le \theta \le 0^-, \end{cases} \tag{3}$$

and the function Θ_3 for V3 is given by

$$\Theta_3(\theta) = \begin{cases} \alpha_3\theta + \Theta_2(0^+) & \text{if } 0^+ \le \theta \le \dfrac{\pi}{2}, \\ \alpha_3\theta + \Theta_2(0^-) & \text{if } -\dfrac{\pi}{2} \le \theta \le 0^-. \end{cases} \tag{4}$$

The wedge map warps three copies of the visual hemi-field (one each for V1, V2, and V3) and places them into the 'pac-man' shape shown in Fig. 1(e). Each copy has been compressed by an amount α_k in the azimuthal direction, resulting in a *rotational shear* in each of the wedges.

[5] Here $0^+ \equiv 0 + |\epsilon|$ and $0^- \equiv 0 - |\epsilon|$ as $\epsilon \to 0$.

The wedge map is then composed with a dipole map $w = k \log[(z+a)/(z+b)]$ to produce the full *wedge–dipole model*, as shown in Fig. 1(d)–(f). This model provides a good qualitative fit to the data—in Fig. 1(h) and (j) we show the topographic data of Fig. 1(g)–(i), respectively, with the wedge–dipole map superimposed (see caption for parameters).

This model achieves each of the goals outlined in Section 3.1.

(1) The wedge map imposes a constant compressive shear in the azimuthal direction via the angular compression parameters α_1, α_2, and α_3. This results in a compression along the iso-eccentricity curves of the dipole map, inducing a simple form of shear in each of the areas of the wedge–dipole map.
(2) The dipole parameters a and b determine the overall shape of the area borders, and the compression parameters α_1, α_2, and α_3 not only prescribe the shear, but also allow the relative surface areas to be varied to match the data.
(3) The wedge map construction enforces the boundary conditions between adjacent areas—image points of the V1 vertical meridians correspond to image points of the V2 vertical meridian (i.e., $re^{\Theta_1(\pm\pi/2)} = re^{\Theta_2(\pm\pi/2)}$), and likewise image points of the V2 horizontal meridians correspond to image points of the V3 horizontal meridians (i.e., $re^{\Theta_2(0)} = re^{\Theta_3(0)}$).
(4) As $\mathrm{d}\Theta_1/\mathrm{d}\theta$ and $\mathrm{d}\Theta_3/\mathrm{d}\theta$ are positive, and $\mathrm{d}\Theta_2/\mathrm{d}\theta$ is negative (see equations (2)–(4)), the Jacobian of the wedge map, and therefore that of the wedge–dipole map, reverses sign across the borders of adjacent areas.
(5) By construction, the dipole mapping ensures logarithmic spacing of iso-eccentricity lines for the parafoveal representation and the inverse of its derivative is sub-linear for the peripheral representation (Schwartz, 1984).

Note that we are able to jointly model areas V1, V2, and V3 with a single map function, suggesting that *these three areas be considered as a single entity*, the *V1–V2–V3 complex*.

4 Discussion

Sources of topographic data The topographic data shown in Fig. 1(g) and Fig. 1(i) consists of qualitative outlines of topography based on the collective experience of the investigators involved. Unfortunately, there is, at present, very little quantitative topographic data to which we can fit our model.

This is partly due to technical difficulties in collecting full-field visuotopic data: in fMRI experiments, the narrow bore of the magnet makes it difficult to present stimuli in the visual periphery. In addition, the unreliability of quantitative topographic data is exemplified by the wide variation in the

reported measurements of $\log(z + a)$ parameter a with little error analysis (Wilson et al., 1990).

Furthermore, it has become common practice to make cuts in cortex that run *through* the V1–V2–V3 complex (in particular through the base of the calcarine fissure, which corresponds to the representation of the horizontal meridian in V1), prior to flattening (e.g. see Kaas, 1998). These cuts drastically alter the topology of this region of cortex, resulting in flatmaps that need to be deformed and 'glued' back together in order to observe the structure of their topography.

Other forms of shear In this paper, we have assumed a very simple form for the topographic shear. A constant rotational shear is produced by the wedge map in each area, i.e. a compression along iso-eccentricity lines. There is evidence that this is not a good assumption for V1, where there appears to be a significant amount of shear near the representation of the vertical meridian but less near the representation of the horizontal meridian (Blasdel and Campbell, 2001; LeVay et al., 1975; van Essen et al., 1984; Tootell et al., 1982; Schwartz, 1994).

It has been hypothesized (Tootell et al., 1982; Blasdel and Campbell, 2001) that topographic shear in V1 is related to the injection of two full representations of the visual field (left and right hemi-retinae) into the ocular dominance columns (ODCs) in V1. Hoever, this idea fails to explain the deficit of shear at the horizontal meridian representation, where ocular dominance columns are well organized over small distances. Nevertheless, a more realistic assumption would be to have the shear follow ODC boundaries, rather than iso-eccentricity lines. Similarly, the shear in V2 could be induced to follow the boundaries of the thick–thin–interstripe columns. We plan to investigate these more sophisticated models in future work.

Quasiconformal mapping A topographic map exhibiting an anisotropic magnification (e.g. the wedge–dipole map) is a *quasiconformal mapping* (Ahlfors, 1966b), meaning that its deviation from a purely conformal mapping is bounded. [6] As conformality is a geometric property that is derived from the imposed metric, every continuous quasiconformal mapping can be shown to be conformal with respect to a specific metric (see, for example, Ahlfors, 1955; Ahlfors and Bers, 1960).

Given a specification of the shear present in a mapping (e.g. the wedge map or the shear patterns described in Section 4), one can extract the shear deformation from the mapping Jacobian. [7] It is then possible to compute a mapping function that is conformal with respect to the new metric, using either complex-analytic functions (as in this paper) or numerical conformal methods (as in the use of Symm's algorithm by Frederick and Schwartz (1990)). Finally, one can re-insert the shearing deformation into the metric

[6] Although the derivative of a conformal or quasiconformal map must be non-zero, the derivative of the wedge map is zero at the origin. However, this critical point is isolated.

to arrive at the full quasiconformal mapping. Thus, generalizations of shear patterns can be combined with generalizations of conformal mappings to produce a rich class of models that can be used to model visual topography.

Visual areas V3, MT, and DL There has been some question as to whether the cortical area adjacent to V2 on its outer boundary constitutes a single area, V3, or whether it constitutes two different visual areas: VP and V3d (see Kaas, 1998, for a review). However, recent studies have provided convincing support for a single V3 representation (Lyon and Kaas, 2001, 2002), and the V1–V2–V3 complex is consistent with this idea.

Another example of a cortical complex is in the owl monkey, where visual areas MT and DL bear a superficial resemblance to a V1–V2 complex (see Fig. 1(i)), which suggests that this MT–DL complex may also be modeled with the techniques presented in this paper.

Singularities of cortical maps The dipole mapping $w = k \log[(z+a)/(z+b)]$ introduces two singularities at $z = -a$ and $z = -b$ on the negative real axis. As more visual areas are included into the wedge map construction, the domain of the dipole mapping begins to approach the singularities, i.e. the 'pac-man' in Fig. 1(e) begins to close down onto the negative real axis as more 'wedges' (i.e. visual areas) are added to the complex. Another way to see this is to consider modeling V1 and V2 with no rotational compression: the domain of each area would occupy a half-disc, thus the dipole domain would include the entire disc and the singularities on the negative real axis would therefore be unavoidable.

This provides an interpretation of the need for shear in the wedge–dipole model: without rotational compression, the V2 wedge would encounter the logarithmic singularities. The consequence, which we have observed in computer simulation, is that the surface area of V2 diverges if the domain of V2 is allowed to approach the negative real axis in the wedge map. Rotationally shearing V2 compresses the domain of the dipole mapping away from the negative real axis. Thus, the existence of large shear in V2 and V3 in cortex may be a side-effect of the nature of topographic map singularities, together with the observed boundary conditions (i.e. field reversal, shared boundaries, etc.). Avoidance of these singularities may help define the global geometric structure of the cortical topography by regulating the amount of shear and the total area for each region. Under the assumptions of the wedge–dipole model listed in Section 3.1, there is a trade-off between area and shear such that no more than three or four regions can be represented in a single complex without requiring either very large shear or very

[7] The differential, or Jacobian matrix, of a regular map $f : \mathbb{R}^2 \to \mathbb{R}^2$ is represented by a combination of a dilation (the trace), a rotation (the anti-symmetric component), and a deformation or shear (the traceless symmetric component). If a map is conformal (i.e., isotropic), its shear component is zero. See (Schwartz, 1984, 1994) for detailed discussion in the present context, or, for the original discussion, see (von Helmholtz, 1858).

small area.

Steady state diffusion source and sink The real part of the *ab*-dipole map is the steady state solution to the diffusion equation

$$\nabla^2\phi - \frac{\mathrm{d}\phi}{\mathrm{d}t} = \delta(x+a,y) - \delta(x+b,y) \tag{5}$$

for a single source and sink, and the imaginary part is given by its harmonic conjugate (Needham, 1997). From this point of view, it is a 'natural' model function to represent two-dimensional patterns. It would appear that developmental modeling, in terms of gradients of morphogenetic or other chemo-tactic control, might benefit from the analysis of this paper. The results of this paper suggest that it may be possible to developmentally code for the topographic structure of visual cortex using a sheared dipole architecture specified by a small number of parameters.

Acknowledgments

We thank Michael Cohen and Robert Ajemian for helpful comments and discussion.

References

Ahlfors, L. V., 1955. Conformality with respect to Riemannian metrics. Annales Academi Scientiarum Fennicæ Series A. I. Mathematica (206), 1–22.

Ahlfors, L. V., 1966a. Complex analysis: an introduction to the theory of analytic functions of one complex variable, 2nd Edition. McGraw-Hill, New York.

Ahlfors, L. V., 1966b. Lectures on quasiconformal mappings. Van Nostrand, Princeton, N.J., manuscript prepared with the assistance of Clifford J. Earle, Jr.

Ahlfors, L. V., Bers, L., 1960. Riemann's mapping theorem for variable metrics. Annals of Mathematics 72, 385–404.

Allman, J. M., Kaas, J. H., 1975. The dorsomedial cortical visual area: A third tier area in the occipital pole of the owl monkeys (*Aotus trivirgatus*). Brain Research 100, 473–487.

Blasdel, G., Campbell, D., 2001. Functional retinotopy of monkey visual cortex. Journal of Neuroscience 21 (20), 8286–8301.

Daniel, M., Whitteridge, D., 1961. The representation of the visual field on the cerebral cortex in monkeys. Journal of Physiology 159, 203–221.

DeYoe, E. A., Carman, G. J., Bandettini, P., Glickman, S., Wieser, J., Cox, R., Miller, A., Neitz, J., 1996. Mapping striate and extrastriate visual areas

in human cerebral cortex. Proceedings of the National Academy of Sciences - USA 93 (6), 2382–2386.

Dow, B., Vautin, R. G., Bauer, R., 1985. The mapping of visual space onto foveal striate cortex in the macaque monkey. Journal of Neuroscience 5, 890–902.

Engel, S. A., Glover, G. H., Wandell, B. A., Mar. 1997. Retinotopic organization in human visual cortex and the spatial precision of functional MRI. Cerebral Cortex 7 (2), 181–192.

Frederick, C., Schwartz, E. L., Mar. 1990. Conformal image warping. IEEE Computer Graphics and Applications 10, 54–61.

Horton, J. C., Hoyt, W. F., 1991. Quadrantic visual field defects: a hallmark of lesions in extrastriate (V2/V3) cortex. Brain 114, 1703–1718.

Kaas, J. H., 1998. Theories of visual cortex organization in primates. In: Rockland et al. (1998), Ch. 3, pp. 91–125.

LeVay, S., Hubel, D. H., Wiesel, T. N., 1975. The pattern of ocular dominance columns in macaque visual cortex revealed by a reduced silver stain. Journal of Comparative Neurology 159, 559–576.

Lyon, D. C., Kaas, J. H., 2001. Connectional and architectonic evidence for dorsal and ventral V3, and dorsomedial area in marmoset monkeys. Journal of Neuroscience 21, 249–261.

Lyon, D. C., Kaas, J. H., Jan. 2002. Evidence for a modified V3 with dorsal and ventral halves in macaque monkeys. Neuron 33, 453–461.

Needham, T., 1997. Visual Complex Analysis. Oxford University Press, New York.

Rockland, K. S., Kaas, J. H., Peters, A. (Eds.), 1998. Cerebral Cortex. Vol. 12: Extrastriate Cortex in Primates. Kluwer Academic/Plenum Publishers, New York.

Roe, A. W., Ts'o, D. Y., 1998. The functional architecture of area V2 in the macaque monkey: Physiology, topography, and connectivity. In: Rockland et al. (1998), Ch. 7, pp. 295–333.

Rojer, A. S., Schwartz, E. L., 1990. Design considerations for a space-variant visual sensor with complex-logarithmic geometry. 10th International Conference on Pattern Recognition, Vol. 2 , 278–285.

Rosa, M. G. P., Sousa, A. P. B., Gatass, R., 1988. Representation of the visual field in the second visual area of the *Cebus* monkey. Journal of Comparative Neurology 275, 326–345.

Schwartz, E. L., 1977. Spatial mapping in primate sensory projection: analytic structure and relevance to perception. Biological Cybernetics 25, 181–194.

Schwartz, E. L., 1980. Computational anatomy and functional architecture of striate cortex: a spatial mapping approach to perceptual coding. Vision Research 20, 645–669.

Schwartz, E. L., 1983. Cortical anatomy and size invariance. Vision Research 18, 24–58.

Schwartz, E. L., 1984. Anatomical and physiological correlates of human visual perception. IEEE Transactions on Systems, Man and Cybernetics SMC-14,

257–271.

Schwartz, E. L., 1985. On the mathematical structure of the retinotopic mapping of primate striate cortex. Science 227, 1066.

Schwartz, E. L., Apr. 1994. Computational studies of the spatial architecture of primate visual cortex: Columns, maps, and protomaps. In: Peters, A., Rockland, K. S. (Eds.), Cerebral Cortex. Vol. 10: Primary Visual Cortex in Primates. Kluwer Academic/Plenum Publishers, New York, pp. 359–411.

Sereno, M., Dale, A., Reppas, J., Kwong, K., Belliveau, J., Brady, T., Rosen, B., Tootell, R., 1995. Borders of multiple visual areas in humans revealed by functional MRI. Science 268, 889–893.

Symm, G. T., 1966. An integral equation method in conformal mapping. Numerische Mathematik 9, 250–258.

Tootell, R. B., Silverman, M., Switkes, E., DeValois, R., 1982. Deoxyglucose analysis of retinotopic organization in primate striate cortex. Science 218, 902–904.

Tootell, R. B., Silverman, M. S., Switkes, E., DeValois, R., 1985. Deoxyglucose, retinotopic mapping and the complex log model in striate cortex. Science 227, 1066.

van Essen, D. C., Newsome, W. T., Maunsell, J. H. R., 1984. The visual representation in striate cortex of the macaque monkey: Asymmetries, anisotropies, and individual variability. Vision Research 24, 429–448.

von Helmholtz, H., 1858. Über integral der hydronamischen gleichungen, welche den wirbelbewegungen entsprechen. Crelle's Journal für Mathematik 55, 25–55, English translation by P. G. Tait, *Philosophical Magazine and Journal of Science* 4th Ser., supplement to vol 33, June 1867, 485-511.

Wilson, H., Levi, D., Maffei, L., Rovamo, J., DeValois, R., 1990. The perception of form: Retina to striate cortex. In: Spillman, L., Werner, J. S. (Eds.), Visual Perception: The Neurophysiological Foundations. Academic Press, New York, Ch. 10, pp. 231–272.

Wolfson, E., Schwartz, E. L., 1989. Computing minimal distances on arbitrary polyhedral surfaces. IEEE Transactions on Pattern Analysis and Machine Intelligence 11, 1001–1005.